A facile preparation of CuS-BSA nanocomposite as enzyme mimics: Application for selective and sensitive sensing of Cr(VI) ions

Abir Swaidan, Priyakshree Borthakur, Purna Boruah, Manash R. Das, Alexandre Barras, Salah Hamieh, Joumana Toufaily, Tayssir Hamieh, Sabine Szunerits, Rabah Boukherroub

A facile preparation of CuS-BSA nanocomposite as enzyme mimics: Application for selective and sensitive sensing of Cr(VI) ions

Abir Swaidan,[a,b] Priyakshree Borthakur,[c,d] Purna K Boruah,[c,d] Manash R Das,[c,d] Alexandre Barras,[a] Salah Hamieh,[b] Joumana Toufaily,[b] Tayssir Hamieh,[b] Sabine Szunerits[a] and Rabah Boukherroub[a*]

[a] *Univ. Lille, CNRS, Centrale Lille, ISEN, Univ. Valenciennes, UMR 8520 - IEMN, F-59000 Lille, France*

[b] *Univ. Libanaise, LEADDER, Laboratoire des études appliquées au développement durable et énergie renouvelable, Hadath, Liban*

[c]*Advanced Materials Group, Materials Sciences and Technology Division, CSIR-North East Institute of Science and Technology, Jorhat-785006*

[d]*Academy of Scientific and Innovative Research, CSIR-NEIST Campus, India*

*To whom correspondence should be addressed: Rabah Boukherroub, e-mail: rabah.boukherroub@univ-lille.fr; Tel: +333 62 53 17 24

Abstract

This work describes a selective and sensitive colorimetric approach for the detection of heavy metal Cr(VI) ions in water using the peroxidase-like property of CuS-BSA nanocomposite. CuS-BSA nanocomposite is synthesized *via* a simple chemical route and characterized by various sophisticated instrumental techniques like transmission electron microscopy (TEM), Fourier transform infrared spectroscopy (FTIR), UV/Vis absorption spectroscopy, X-ray photoelectron spectroscopy (XPS), and thermogravimetric analysis. The hydrodynamic size and surface charge of CuS-BSA nanocomposite were determined by using dynamic light-scattering (DLS) and zeta potential measurements. The peroxidase-like activity of CuS-BSA nanocomposite towards the catalytic oxidation of 3,3′,5,5′-tetramethylbenzidine (TMB) in the presence of H_2O_2 to produce a blue colored charge transferred oxidized product (oxTMB), which is observable by the naked eye, is quantitatively assessed by UV/vis spectrophotometry at 654 nm. The CuS-BSA nanocomposite is subsequently applied for sensing of Cr(VI) metal ions. The sensor displays two linear ranges, 0-100 nM and 1-20 μM; the lower linear range was used to determine a detection limit of 50 nM towards Cr(VI), which is below the permissible limit determined by the United States Environmental Protection Agency (U.S. EPA). The practical performance of this sensor is successfully demonstrated using various environmental water samples spiked with different concentrations of Cr(VI). This method offers the advantages of being rapid, highly selective and sensitive platform, which holds great potential in environmental applications.

Key words: *CuS-BSA; Peroxidase mimic; Cr(VI) ions; Colorimetric; Detection.*

1. Introduction

Contaminated water by heavy metal ions represents a major risk to human health. Although most of heavy metal ions are essential to human body, when their concentration exceeds the normal level, they cause chronic toxicities. Thus, the detection of metal ions in water is a persistent need for environmental protection.

Chromium generally occurs in the environment in two main forms: Cr(VI) and Cr(III). Cr(III) is considered as an essential element for carbohydrate, protein and lipid metabolism, as well as insulin efficiency [1] due to its enhancement in transporting glucose through the cell membrane. Indeed, supplemental Cr(III) as chromium picolinate enhances the blood glucose, insulin, hemoglobin and cholesterol in a concentration dependent way in Type 2 diabetes mellitus. In contrast, deficiency in Cr(III) can result in nerve and brain damage. The first report to highlight chromium deficiency was in 1977 [2], when a patient suffered from low insulin levels due to glucose intolerance, where it has been observed that Cr requirement is closely related to the level of glucose metabolism. Unlike Cr(III), Cr(VI) is highly toxic and considered to be carcinogen [3]. This form of chromium compound can be found in the earth's crust and used in many industrial processes such as chrome plating, manufacturing of pigments and dyes, paints, plastics, wood preservation, and leather tanning [4]. Therefore, the risk of Cr(VI) disposal to water, air, and soil is restricted to means of industrial facilities. The high solubility and mobility of anionic forms of Cr(VI) ($HCrO_4^-$ or CrO_4^{2-}) raised concern on the hazardous effect of these species. Indeed, Cr(VI) ions can be also transported through cellular membranes by sulphate/phosphate anion channels due to their similarity in structure, since at physiological pH, hexavalent chromium exists as oxyanion with an overall -2 charge [5]; once inside the cells, it can interact with biological species (ex. DNA) [6], causing extensive damage and leading to serious deficiencies.

On the other hand, H_2O_2, a naturally occurring by-product of oxygen metabolism, is of biological interest, due to its ability to transform into harmful free radicals that can readily interact with biological molecules. Recently, it has been found that H_2O_2 can form an intermediate with thiol-group containing species in the cellular membrane for the activation of Cr(VI) ions to enhance their toxicity and mutagenicity [7]. The interaction between H_2O_2 and

Cr(VI) ions is demonstrated to be pH-dependent. Joaquin *et al.* [7] reported that at low pH, Cr(VI) acts as an oxidizing agent towards the generation of hydroxyl radicals.

The U.S. EPA (Environmental Protection Agency) Guidelines for Carcinogen Risk Assessment [8, 9], stated that Cr(VI) concentration in drinking water exceeding 0.1 mg/L is considered to be carcinogen through mutagenic mode of action. Thus, people residing near sources of industrial waste of Cr(VI) compounds and consuming Cr(VI) in drinking water are more susceptible to cancer. Therefore, it is mandatory to develop a highly efficient technique for Cr(VI) detection.

Many methods have been reported for efficient sensing of heavy metal ions, such as atomic absorption [10], emission [11], and mass spectroscopies [12]. Although these methods are highly selective and sensitive for detecting heavy metal ions, they are time-consuming, require specialized equipment and cannot be applied for real-time or field analysis. Thereby, the colorimetric detection holds interest due to its simplicity, low cost, fast response, and low detection limit.

With the emergence of nanotechnology, the development of enzyme mimics as colorimetric biosensors offers great advantages in the environmental and biomedical fields. In 2007, Gao et al. [13] demonstrated the use of ferromagnetic Fe_3O_4 nanoparticles (NPs) that possess enzyme-like activity similar to the naturally occurring horseradish peroxidase enzyme (HRP). Since then, a tremendous amount of efforts has been devoted to the preparation of a plethora of enzyme-like nanomaterials (commonly designed as nanoenzymes) for sensing of H_2O_2, glucose and other biologically relevant molecules [14].

In recent years, semiconductor chalcogenides and particularly copper sulfide (CuS) nanostructures have received tremendous interest, owing to their high abundance, low cost, and unique electronic and optical properties. These materials have found widespread use in various fields like photovoltaics, photocatalysis, energy conversion devices, biosensors, etc. [15]. However, in absence of appropriate surface coating, these nanostructures tend to agglomerate in aqueous media, hampering their applications [16].

Many studies reported that biomolecules such as proteins can be used to prevent nanomaterial's aggregation [17]. Therefore, great efforts have been made to develop peroxidase mimics with excellent stability. The high water solubility and stability of bovine serum albumin

(BSA) protein, as well the presence of various binding sites in its structure, makes it a key factor to stabilize CuS NPs and prevent their aggregation to enhance their sensing performance.

Herein, BSA was used as a template to synthesize water dispersible copper sulfide nanoparticles (CuS NPs) *via* a facile method. The obtained CuS-BSA nanocomposite was applied for selective Cr(VI) colorimetric sensing. The as-synthesized CuS-BSA nanocomposite exhibited good stability and dispersibility in various aqueous media and displayed intrinsic peroxidase-mimic for efficient catalytic oxidization of 3,3′,5,5′-tetramethylbenzidine (TMB) substrate in the presence of H_2O_2. This property was further exploited for the detection of Cr(VI) in acidic aqueous medium, as confirmed by a naked eye detection of the color change of the solution from transparent to blue. Additionally, UV/vis absorbance spectroscopy was used for the quantitative determination of the oxidized TMB (oxTMB) at 654 nm. The mechanism of TMB oxidation was enhanced by H_2O_2 decomposition by Cr(VI) to generate $HO^{\bullet}$ in the presence of CuS-BSA. The experimental parameters for colorimetric Cr(VI) detection including temperature, pH and incubation time were also assessed. A detection limit of Cr(VI) as low as 50 nM was achieved under optimized conditions.

2. Experimental section

2.1. Materials and Methods

Bovine serum albumin (BSA, ≥ 96%), copper(II) acetate [$Cu(Ac)_2$, 98.0%], sodium sulfide hydrate ($Na_2S.xH_2O$, ≥ 97.0%), sodium hydroxide pellets (NaOH, ≥ 97.0%), 3,3',5,5'-tetramethylbenzidine (TMB, ≥ 95.0%), sodium acetate (anhydrous) [CH_3COONa, ≥ 99.0%], chromium(III) chloride hexahydrate ($CrCl_3 \cdot 6H_2O$, 96.0%), chromium trioxide (CrO_3, ≥ 99.0%), nickel(II) chloride hexahydrate ($NiCl_2.6H_2O$, ≥ 98.0%), cobalt(II) nitrate hexahydrate ($CoN_2O_6.6H_2O$, ≥ 98.0%), mercury(II) nitrate monohydrate ($HgN_2O_6.H_2O$, ≥ 99.99%), sodium sulfite (Na_2SO_3, ≥ 98.0%), zinc chloride ($ZnCl_2$, ≥ 98.0%), iron(III) chloride ($FeCl_3$, ≥ 99.99%), and terephthalic acid (C_6H_4-1,4-$(CO_2H)_2$, 98.0 %) were purchased from Sigma-Aldrich. Ethanol (95% v/v), dimethyl sulfoxide (DMSO, ≥99.9%), glacial acetic acid (99.0 %), and hydrogen peroxide (30 wt%, H_2O_2) were purchased from fisher scientific. Milli-Q (MQ) water was used throughout the whole procedure.

2.2. Sample preparation *via* mineralization approach

The CuS-BSA nanocomposite was prepared *via* mineralization process according to a previous procedure [18] with some modifications. In short, an aqueous solution of BSA was prepared by dissolving 250 mg of BSA in 9 mL MQ-water. Then 1.0 mL of $Cu(Ac)_2$ (0.1 M) was added dropwise to the above solution under magnetic stirring, resulting in a blue cloudy mixture, after which a light green color was observed. 0.5 mL of an aqueous NaOH (2.0 M) solution was used to adjust the pH at 12, after which the mixture turned directly to purple. Then 52.0 mg of Na_2S (0.4 M) were added under stirring; the color of the solution turned to brown immediately. The mixture was further processed at 55 °C for 5 h to give a green solution. The resulting CuS-BSA nanocomposite was purified by dialysis against a 12-14 kDa molecular mass cut off dialysis membrane in MQ-water for 24 h to remove excess copper ions (to exclude their contribution in the catalytic process), then stored at 4 °C for later use. A fluffy-like dark green powder of CuS-BSA was collected by lyophilization for further characterization, which can be redispersed easily in MQ-water.

2.3. Peroxidase-mimic based on CuS-BSA nanocomposite

The catalytic activity of CuS-BSA as a peroxidase-mimic was assessed *via* the oxidization of TMB substrate in presence of H_2O_2. In brief, the reaction was carried out first by mixing 150 µL of each TMB (1.6 mM dissolved in 96% ethanol), H_2O_2 (200 mM), and the as-prepared CuS-BSA nanocomposite (1 mg/mL) at a temperature of 25 °C for 25 min. 0.1 M acetate buffer (pH=3.9) was used to adjust the reaction volume to 1.5 mL. Absorption spectra were recorded by UV/vis absorption spectrophotometer in the 350-850 nm range to follow the changes of the oxidized TMB (oxTMB) peak at 654 nm.

The effect of CuS-BSA concentration over the range 0.03-0.20 mg/mL, pH (2.5-10.0), temperature (25-50 °C), and incubation time (0-30 min) were performed to investigate their influence on the catalytic oxidation reaction.

A set of control experiments were also conducted to highlight the catalytic activity of CuS-BSA towards the oxidation of TMB.

2.4. Kinetic analysis of CuS-BSA peroxidase-like activity and determination of the Michaelis-Menten constant and maximum velocity

Enzyme affinity to its substrate can be assessed by the determination of the Michaelis–Menten constant (K_m), where smaller K_m value indicates a high affinity.

A Lineweaver-Burk double reciprocal plot is used to determine the enzyme affinity using the following relation (1):

$$1/V = (K_m/V_{max})\ (1/[S]) + 1/V_{max} \qquad (1)$$

Where V corresponds to the initial rate of the reaction, V_{max} represents the maximum rate, K_m is the Michaelis–Menten constant, and $[S]$ is the concentration of the substrate.

The kinetic measurements were recorded at 654 nm in a time-scan mode at different concentrations of one substrate (TMB or H_2O_2) and at a fixed concentration of the other. The experiments were performed by mixing different concentrations of TMB (0.01-0.16 mM) with H_2O_2 (20 mM) and CuS-BSA (0.1 mg/mL) catalyst in 1.5 mL acetate buffer (0.1 M) at pH 3.9. Similarly, using H_2O_2 as a substrate, the reaction was executed by mixing different concentrations of H_2O_2 (5-20 mM) with TMB (0.16 mM) and CuS-BSA (0.1 mg/mL) in 1.5 mL of 0.1 M acetate buffer (pH=3.9).

2.5. Colorimetric sensing of Cr(VI) in aqueous medium

The colorimetric detection of Cr(VI) ion was carried out by adding various concentrations of CrO_3 (dissolved in water) to a mixture of CuS-BSA (0.1 mg/mL), TMB (0.16 mM), and H_2O_2 (20 mM). The reaction volume was adjusted by 0.1 M acetate buffer (pH = 3.9) to 1.5 mL. The resulting mixture was incubated for 25 min at 25 °C, and the absorption spectra were measured by monitoring the absorbance at 654 nm.

Cr(VI) detection was also recorded in the absence of H_2O_2 under the same conditions mentioned above.

2.6. Selectivity and reproducibility

The selectivity of CuS-BSA was investigated for speciation of Cr(VI). The credibility of this assay was studied by determining the absorbance at 654 nm in presence of different potentially

co-existing ions. Thus, 20 µM and 100 µM of different ions (Na^+, Hg^{2+}, Zn^{2+}, Co^{2+}, Ni^{2+}, Cr^{3+}) were mixed with CuS-BSA (0.1 mg/mL), TMB (0.16 mM), and H_2O_2 (20 mM) in 0.1 M acetate buffer (pH = 3.9) to examine the response of the proposed sensor for the colorimetric detection of Cr(VI) ion using other ions at same and five-times higher than the concentration of Cr(VI). The reusability of the nanocomposite was also determined for several repeated cycles under the optimized experimental conditions.

2.7. Mechanism of CuS-BSA catalytic activity in the formation of hydroxyl radicals (HO•)

In order to confirm the catalytic activity of CuS-BSA towards TMB oxidation through the formation of hydroxyl radicals from H_2O_2 decomposition in acidic medium, terephthalic acid (TA) was used as a probe molecule that can readily react with •OH radicals to produce 2-hydroxyterephthalic acid (HTA). The HTA exhibits a fluorescence emission peak at 430 nm under excitation wavelength of 315 nm. In brief, TA (0.15 mM in DMSO) was subsequently treated with (a) H_2O_2 (20 mM), (b) Cr (VI) (20 µM), (c) CuS-BSA (0.1 mg/mL), (d) H_2O_2 (20 mM) + CuS-BSA (0.1 mg/mL), (e) H_2O_2 (20 mM) + Cr(VI) (20 µM), (f) Cr(VI) (20 µM) + CuS-BSA (0.1 mg/mL), (g) H_2O_2 (20 mM) + Cr(VI) (20 µM) + CuS-BSA (0.1 mg/mL) in 1.5 mL acetate buffer (pH=3.9) and incubated for 25 min at 25 °C. The fluorescence emission spectra were then collected in the range of 325-550 nm using a Safas Xenius XC fluorescence spectrophotometer (Monaco) under excitation wavelength of 315 nm.

2.8. Sensing of Cr(VI) ion in real environmental water samples

To investigate the practical application of CuS-BSA as a colorimetric sensor, concentration of Cr(VI) ions were determined in various real environmental water samples (sea, pond, tap and tube well water) spiked with different concentrations of Cr(VI) ions. The tube well water samples were taken from local area of Lille city, Rihour, France. The pond water samples were collected from the Parc du Héron, Villeneuve d'Ascq (France). The tap water samples were obtained from our laboratory (IEMN, Villeneuve d'Ascq), and the sea water samples were from the North Sea (marginal sea of Atlantic Ocean). The collected water samples were purified by centrifugation at 13,500 rpm for 10 min and the supernatant was then collected and filtered through 0.2 µm pore size membrane, before standard solutions of Cr(VI) ions (10, 50, 100 nM) were added separately.

The sensing experiments were conducted as follows: 150 µL of the as-prepared CuS-BSA suspension (1 mg/mL), 150 µL of TMB (1.6 mM in ethanol) and 150 µL of H_2O_2 (200 mM) were added successively to 150 µL of each water sample containing different concentrations of Cr(VI) (10, 50, 100 nM), and the total volume was adjusted to 1.5 mL by adding acetate buffer (pH = 3.9). The reaction mixture was kept at 25 °C for 25 min, and the absorbance was monitored at 654 nm by UV/vis absorbance spectrophotometry.

3. Results and discussion

3.1. Characterization of CuS-BSA nanocomposite

The synthesis of CuS-BSA nanocomposite was carried out in two steps, first by forming Cu^{2+}-BSA complex through the addition of $Cu(Ac)_2$ into BSA solution, where Cu^{2+} cations can bind with BSA through exposing the binding sites of BSA to Copper ions in alkaline pH medium (pH 12), followed by the release of S^{2-} by adding Na_2S. The presence of free -SH in cysteine amino acid of BSA [19] enhances the conjugation of metal sulfides to BSA, and acts as a nucleating agent for the formation of CuS-BSA. The formation of CuS-BSA can also be easily visualized by color change, as clearly observed in **Fig. S1**.

The chemical composition of CuS-BSA nanocomposite and BSA precursor was evaluated by X-ray photoelectron spectroscopy (XPS) analysis. The XPS survey spectrum of BSA **(Fig. S2a)** clearly indicates the presence of C_{1s} (285 eV), O_{1s} (532 eV), N_{1s} (400 eV) corresponding to peptide nitrogen, and S_{2p} at 163 eV due to the presence of free thiol (SH). The atomic concentrations of C_{1s}, N_{1s}, O_{1s}, and S_{2p} are 66.43%, 14.53%, 18.52% and 0.52%, respectively. The deconvolution of C_{1s} high resolution spectrum **(Fig. S2b)** showed the contribution of various functional groups at 286.0 eV (C-O/C-N), and 287.7 eV due to carbonyl carbon (C=O/C=N), a peak at 284.7 eV ascribed to the aliphatic carbon [20, 21], and the C–S bond of cysteine [22] in BSA. The high resolution N_{1s} spectrum can be fitted with two bands attributed to C=N [23] and C-N [24] at around 397.5 and 400.0 eV, respectively **(Fig. S2c)**. The O_{1s} spectrum **(Fig. S2d)** can be fitted with one symmetrical peak at 531.0 eV due N-C=O and OH in BSA [20]. In the S_{2p} high resolution XPS spectrum **(Fig. S2e)**, the peaks at 163 and 168 eV are attributed to SH [25] and SO_4^{2-}, respectively. SO_4^{2-} originates most likely from partial sulfur oxidation under ambient conditions.

The XPS survey spectrum of CuS-BSA **(Fig. 1a)** comprises bands attributed to C_{1s} (285 eV), N_{1s} (400 eV), O_{1s} (532 eV), Cu_{2p} (932 eV) and S_{2p} (163 eV) with atomic concentrations of 62.97%, 15.44%, 19.69%, 0.77% and 1.12%, respectively. The atomic ratio of Cu/S is calculated to be 0.68:1; the deviation from 1 is due to the presence of S groups in BSA.

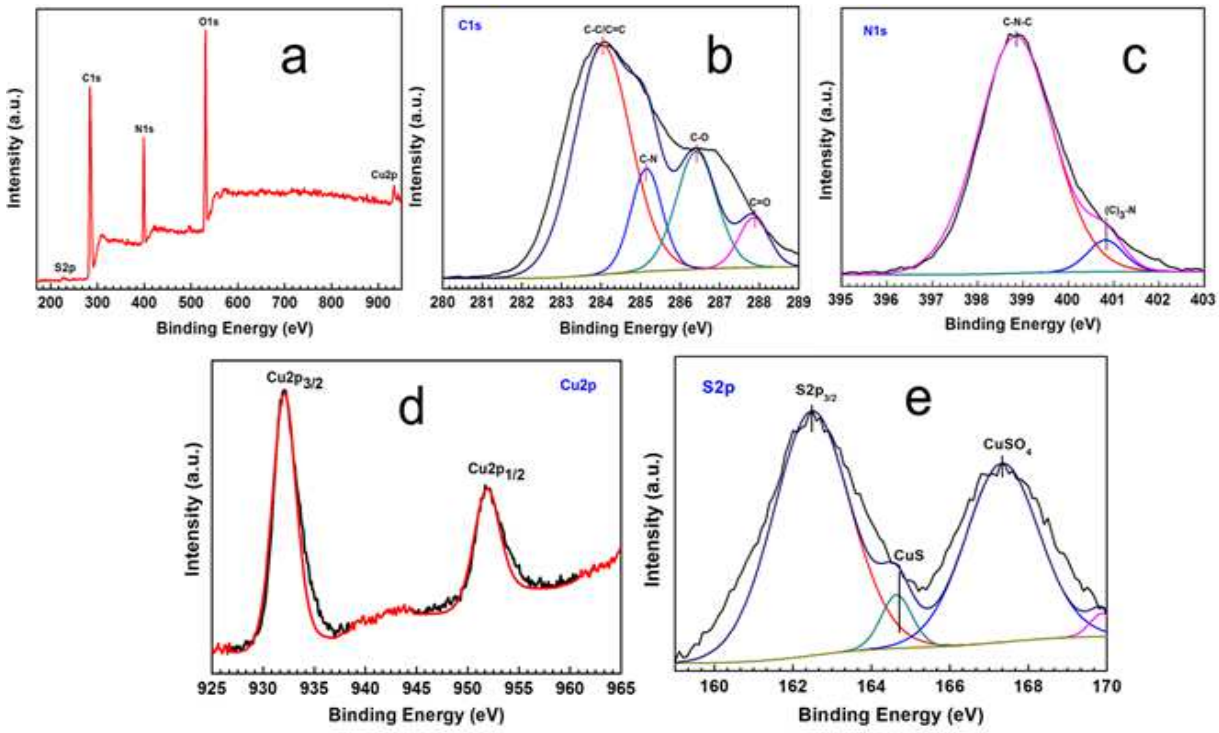

Figure 1: XPS survey spectrum (a), and high resolution XPS spectra of C_{1s} (b), N_{1s} (c), Cu_{2p} (d) and S_{2p} (e) of CuS-BSA nanocomposite.

The C_{1s} high resolution XPS spectrum of CuS-BSA **(Fig. 1b)** can be fitted with several components at binding energies of 284.04, 285.25, 286.41 and 287.86 eV corresponding to C-C/C=C, C-N, C-O and C=O groups, respectively [26, 27]. The C–S bond is not clearly observed because the binding energy of C–S at 285.3 eV is very close to that of sp^3 C–C [28]. Similarly, the N_{1s} high resolution XPS spectrum of CuS-BSA **(Fig. 1c)** can be deconvoluted into C-N-C (398.84 eV) and $(C)_3$-N (400.82 eV) of BSA [29, 30]. This is not surprising since nitrogen contribution originates from BSA only. **Fig. 1d** represents the deconvoluted spectrum of Cu_{2p} with peaks at 932.06 and 951.82 eV assigned to $Cu_{2p3/2}$ and $Cu_{2p1/2}$, respectively. A characteristic

satellite peak is observed at around 943 eV, indicating the presence of paramagnetic Cu^{2+} ions of CuS [31].

In the S_{2p} high resolution XPS spectrum of CuS-BSA (**Fig. 1e**), the peaks at 164.64 and 167.88 eV are attributed to CuS and $CuSO_4$, respectively [32-34] even though one cannot rule out a contribution of oxidized sulfur in BSA. The peak at ~163 eV originates from S_{2p} in BSA.

The morphology, structure and particle size of CuS-BSA nanocomposite were characterized by TEM analysis (**Fig. 2**). TEM images **(Fig. 2a, b)** indicate that CuS-BSA nanocomposite consists

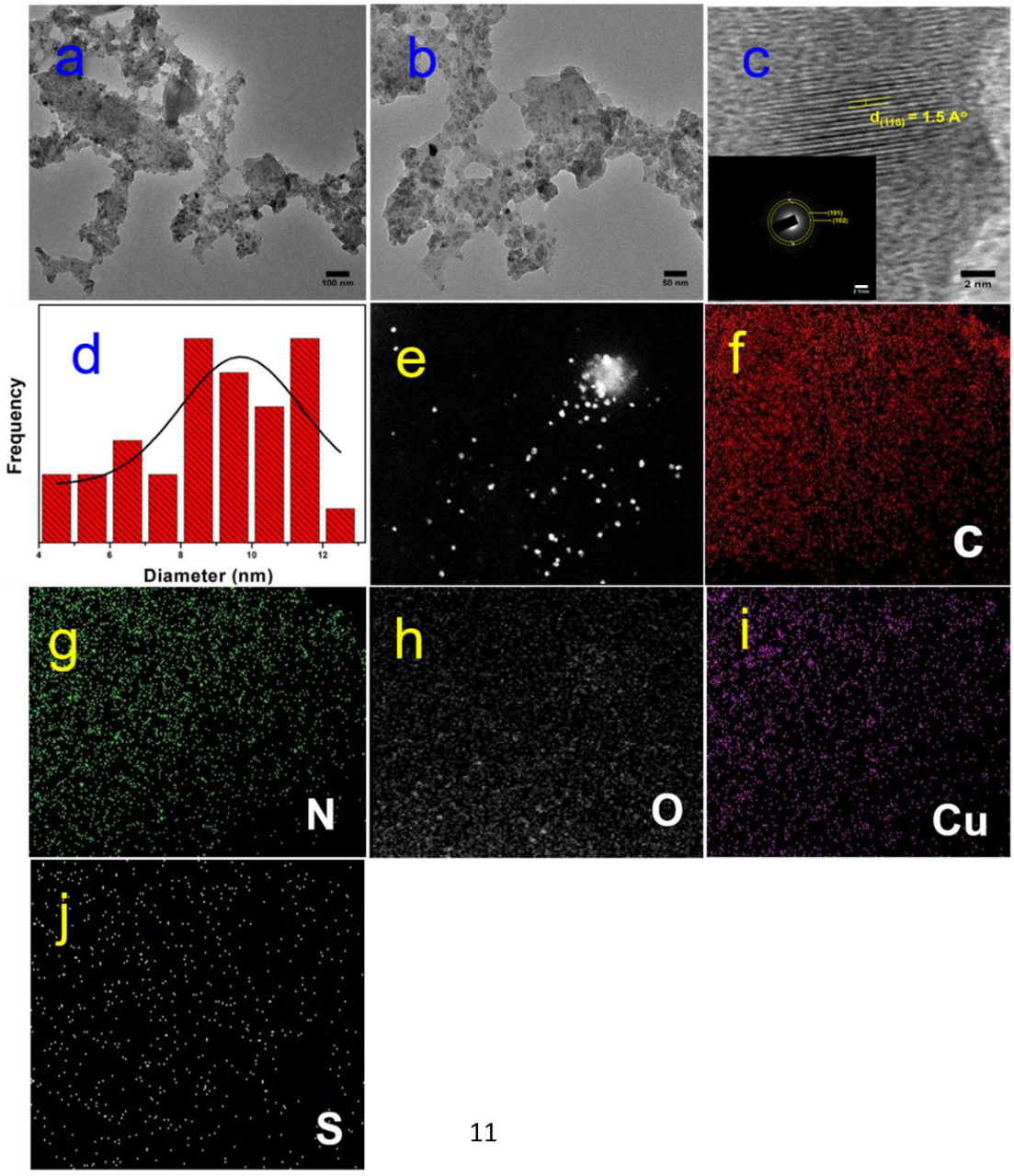

Figure 2: (a, b) TEM images, (c) HRTEM image and SAED pattern (inset), (d) particle size distribution, (e) HAADF-STEM image, elemental mapping for (f) carbon, (g) nitrogen, (h) oxygen, (i) copper, (j) sulfur of CuS-BSA nanocomposite.

of nanoparticles with an average size of 9.7 ± 0.6 nm, as shown in **Fig. 2d** (the size of the NPs was calculated by using Image J software). HRTEM and SAED pattern of the synthesized CuS-BSA nanocomposite revealed good crystallinity of the NPs (**Fig. 2c**). The lattice fringe spacing of CuS-BSA NPs is about 0.15 nm, which corresponds to the (116) plane of CuS nanoparticles. The SAED pattern in the inset of **Fig. 2c** displays the (101) and (102) crystalline planes of CuS, confirming the formation of crystalline CuS-BSA NPs. The elemental mapping confirmed the coexistence of C, N, O, Cu and S elements in CuS-BSA nanocomposite (**Fig. 2 f-j**), in full accordance with the XPS analysis data.

Dynamic light-scattering and zeta potential were used to determine the hydrodynamic size and surface charge of CuS-BSA nanocomposite, respectively. The mean hydrodynamic average diameter of the CuS-BSA was determined to be as 53.8 ± 12.3 nm **(Fig. S3),** which is slightly higher than the mean diameter obtained by TEM due to the hydrodynamic water molecules on the surface of the nanocomposite. The zeta potential of CuS-BSA was recorded by dispersing of CuS-BSA (30 μg/mL) solution in 1 mL MQ-water at different pH values adjusted by using NaOH (0.1 M) or HCl (0.1 M). As depicted in **Fig. S4**, CuS-BSA bears a negative charge value of -31.1 ± 5.7 mV due to the presence of -COOH groups in BSA, with an isoelectric point (IEP) of 5.4 at which the surface zeta potential is zero **(Fig. S5)**.

CuS-BSA aqueous solution was stable for five months at a concentration ~10 mg/mL with no noticeable precipitates, which indicates the long-term colloidal stability and dispersibility of our nanocomposite. The long-term stability of CuS-BSA nanocomposite was also examined in different solvents (phosphate buffer saline (PBS), acetate buffer, DMSO, Dulbecco's modified Eagle's medium (DMEM)), where no apparent precipitation was observed at a concentration of 1 mg/mL (**Fig. 3**). Therefore, BSA proved to be an excellent capping agent to prevent aggregation of CuS NPs.

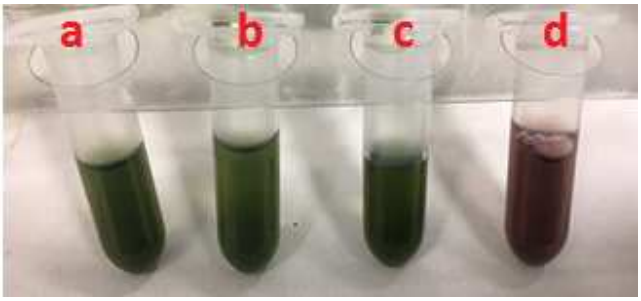

Figure 3: The long-term stability of CuS-BSA (1 mg/mL) dispersed in different solvents (left to right: PBS (a), sodium acetate buffer (b), DMSO (c), and DMEM (d) medium) for one month.

The chemical composition of BSA and CuS-BSA was further assessed by Fourier transform infrared spectroscopy (FTIR). **Fig. 4** displays the FTIR spectrum of pure BSA, comprising the characteristic bands of amide I (C=O) and amide II (C-N stretching or N-H bending vibrations) at 1655 and 1539 cm^{-1}, respectively, OH at 3445-3296 cm^{-1} and amide A (-NH) at 3061 cm^{-1} [17]. The same bands appear in the FTIR spectrum of CuS-BSA, suggesting the presence of BSA in the nanocomposite [35]. However, by comparing both spectra, one can notice a slight decrease of the intensity of the characteristic -NH peak in CuS-BSA most likely due to the coupling between NH in BSA and Cu^{2+}. Additionally, the OH peak in the FTIR spectrum of CuS-BSA is shifted by 49 cm^{-1} [36], confirming the interaction between BSA and CuS, as BSA can provide various binding sites such as -NH, -OH, COOH, and -SH functionalities.

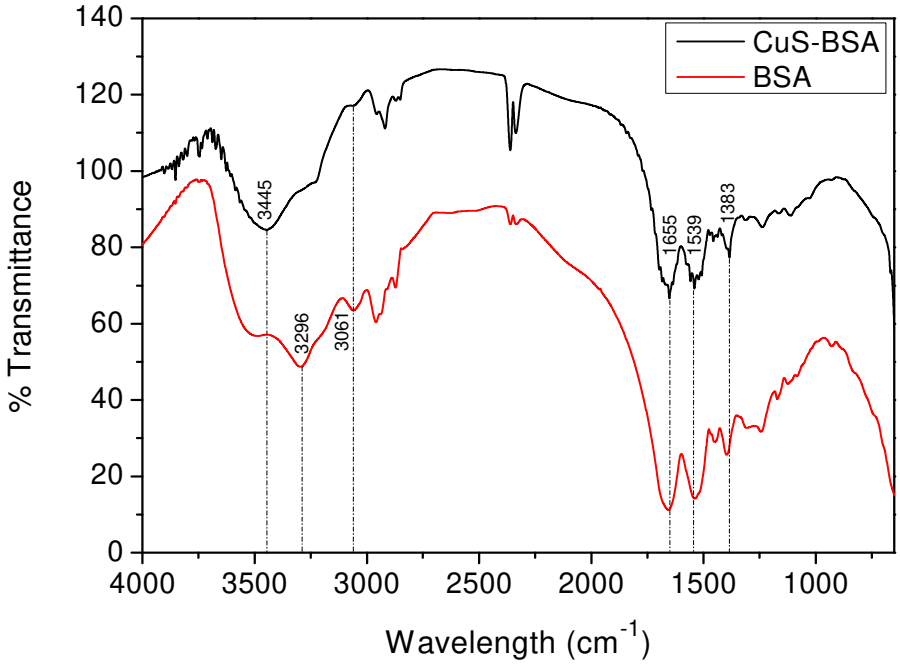

Figure 4: FTIR spectra of native BSA and CuS-BSA nanocomposite.

The UV-Vis absorption spectrum of BSA depicts an optical absorption peak at 280 nm [17]. The same peak appears in the absorption spectrum of CuS-BSA nanocomposite, indicating the growth of CuS on BSA surface. Furthermore, the absorption spectrum of CuS-BSA shows an increase in absorption tail in the near-infrared (NIR) region [37], which is a fundamental characteristic of CuS nanoparticles that absorb light in the NIR range (**Fig S6**).

Thermogravimetric analysis (TGA) and derivative thermogravemetric (DTG) were conducted to confirm the interaction between CuS NPs and BSA and to study their thermal behavior. DTG is performed to detect the slight changes in weight that cannot be observed by TGA. The TGA curve of CuS-BSA exhibited a total weight loss ca. 78.88% from room temperature (RT) to 980 °C **(Fig. S7)**, with 21.12 % of residual mass left at the end of heating, while the TGA curve of pure BSA showed a total weight loss ca 82.43% from RT to 980 °C **(Fig. S8)** with 17.57% of residual mass. This decrease in weight loss for CuS-BSA is attributed to the conjugation between BSA and CuS NPs. Pristine BSA showed 3 stages of weight loss observed by DTG, from 30 to 100 °C, 170 to 250 °C, and from 250 to 565 °C. The first stage of weight loss is due to

evaporation of water molecules, while the second mass loss is assigned to BSA degradation (most likely oxygen containing groups). The last step corresponds to the decomposition of amino acid residues, which occurs at higher temperature range [36]. However, after conjugation of BSA with CuS NPs, the thermal curve displayed only two stages of weight loss, from RT to 100 °C, and from 160 to 480 °C. The decrease in decomposition temperature is attributed to the reduction of thermal stability of BSA after hybridization with the nanoparticles. BSA exhibited a steep curve at 320 °C, which is also displayed in CuS-BSA with a slight decrease in temperature. These results indicated the decrease in thermal stability of BSA could be ascribed to the physical adsorption of CuS on BSA rather than chemical interaction.

3.2. Peroxidase-like catalytic activity of CuS-BSA NPs

The peroxidase-like catalytic activity of CuS-BSA in mimicking the naturally occurring horse-radish peroxidase (HRP) enzyme was examined by studying the oxidation of the TMB molecule. As shown in **Fig. S9**, the oxidation of TMB occurred within 30 s when H_2O_2 was added to CuS-BSA catalyst in acidic medium, confirmed by a visual color change from transparent to blue, and by dynamic increase of the absorbance peak at 654 nm. In order to confirm the catalytic nature of the process, control experiments were carried out in the absence of CuS-BSA and H_2O_2, respectively. Surprisingly, the experimental systems without H_2O_2 showed almost a negligible color change, while in absence of CuS-BSA, a slight blue color was observed **(Fig. S10)**, indicating that both CuS-BSA and H_2O_2 are responsible for the generation of blue colored oxTMB.

It is worth to notice that the oxidation of TMB resulted from the hydroxyl radicals ($^{\bullet}OH$) generated from H_2O_2 decomposition in an acidic medium [38], which are catalyzed by Cu^{2+} ions on the CuS-BSA surface, similar to the Fenton reaction [39]. Basically, H_2O_2 degradation is catalytically mediated by Cu^{2+}, in which a reactive intermediate (Cu^{3+}) is formed through the process. Thereby, copper is being progressively cycled between two different oxidation forms (+2 and +3) (**Fig. 5**).

The mechanism of $^{\bullet}OH$ formation can be summarized as follows:

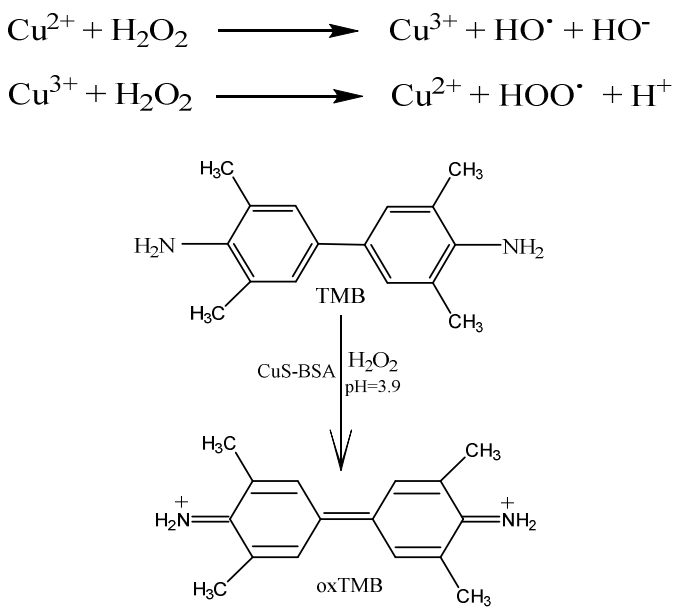

Figure 5: Schematic illustration of the oxidation of TMB.

3.3. Experimental condition optimization

To attain the optimal conditions for the catalytic reaction, TMB oxidation was performed by varying different parameters like the catalyst concentration, solution pH, and temperature of the reaction. The absorbance at 654 nm versus concentration of CuS-BSA response curve was plotted in **Fig. S11**. It is clear that the absorbance gradually increases with the increase of CuS-BSA concentration and saturates at almost 0.1 mg/mL, which is selected for the following experiments. Notably, the rate of the catalytic reaction is highly dependent on catalyst concentration due to the excessive amount of TMB [40].

The catalytic activity of CuS-BSA NPs, like natural enzymes, depends on pH and temperature. Changes of pH (2.5-10) and temperature (25-50 °C) were recorded to demonstrate their influence on the oxidation of TMB. As revealed in **Fig. S12**, the relative activity of CuS-BSA was plotted as a function of temperature, whereby the maximum absorbance intensity at 654 nm was set as 100 %.

Relative activities were determined by the following equation (Eq. 2):

$$R.A = (A654\ nm/A654_{max}) \times 100\ \% \qquad (2)$$

Where R.A represents the relative activity, A654 is to the absorbance of oxTMB at 654 nm, and $A654_{max}$ is the maximum absorbance at 654 nm.

The catalytic oxidation of TMB was stable over a wide temperature range and reaches an optimum intensity at 40 °C, close to the physiological environment, due to the increase in the rate of the enzyme-like reaction at this value. A slight decrease in enzymatic activity takes place at 50 °C, most probably due to partial decomposition of H_2O_2. This result indicates that CuS-BSA displayed better catalytic performance than natural enzymes, which lose their activity completely at high temperature. Similarly, CuS-BSA revealed higher activity at pH 3.9 **(Fig. S13)** due to the enhanced solubility of TMB in acidic environment [40, 41]. Therefore, we performed the following assays in acidic medium and we selected 25 °C for the remaining experiments.

In order to evaluate the rate of the catalytic process, TMB oxidation was monitored at different incubation times in the presence of H_2O_2 (20 mM), CuS-BSA (0.1 mg/mL), and TMB (0.16 mM) in 1.5 mL acetate buffer (pH=3.9). As observed in **Fig. S14**, the catalytic activity of CuS-BSA increased upon increasing the incubation time to reach a maximum value after 25 min; this incubation time was adopted to complete the oxidation reaction in the following experiments.

3.4. Steady-state kinetic mechanism of CuS-BSA as a peroxidase-mimic and determining the Michaelis-Menten constant

The kinetic assay of CuS-BSA as a peroxidase mimic was carried out by determining the initial rate of each substrate, i.e. the slope of ΔA654 per unit time (min). In order to determine the reaction rate of each substrate (TMB and H_2O_2), the UV/vis absorption spectra were recorded at 654 nm in a time-scan mode for different concentrations of substrate **(Fig. S15** and **S17)**. Then the Beer-Lambert law (Eq. 3) was applied to convert the absorbance values to the corresponding concentrations:

$$A = \varepsilon \times c \times l \qquad (3)$$

Where A is the absorbance at 654 nm, ε is the molar absorptivity (ε = 3.9 ×10^4 for oxTMB at 654 nm in $M^{-1}.cm^{-1}$), c represents the concentration of one substrate, and l corresponds to the optical path length (l=1 cm). **Fig. S16** and **S18** depict respectively typical Michaelis–Menten curves for TMB and H_2O_2, where the data are obtained by plotting the initial reaction rate versus concentration of one substrate and changing the concentration of the other. The catalytic parameters (K_m and V_{max}), determined from a Lineweaver–Burk plot, are listed in **Table 1**, where the y-intercept allows to determine the V_{max} and the x-intercept gives the K_m value.

Table 1: Michaelis-Menten constant and maximum velocity for typical TMB and H_2O_2 substrates in comparison with previously reported materials.

Catalyst	K_m (M)		V_{max} ($M.s^{-1}$)	
	H_2O_2	TMB	H_2O_2	TMB
CuS-BSA (our work)	0.014	2 ×10^{-4}	2×10^{-8}	3.3×10^{-8}
HRP [13]	0.0037	4.34×10^{-4}	8.71×10^{-8}	10×10^{-8}
MoS_2 [38]	1.16×10^{-4}	3.87×10^{-4}	2.42×10^{-8}	7.23×10^{-8}
Cu-rGO [42]	0.0263	10.5×10^{-4}	5.385×10^{-8}	3.289×10^{-8}

It was found that the catalytic oxidation of TMB by CuS-BSA follows a typical Michaelis–Menten kinetics, and the low K_m value of CuS-BSA indicates a high affinity towards TMB. The K_m value of CuS-BSA with TMB as the substrate was calculated to be 2×10^{-4} M, which is lower than that of HRP enzyme [43]. However, the K_m value of CuS-BSA with H_2O_2 as substrate is 0.014 M, suggesting a better binding affinity of CuS-BSA to TMB along with a good peroxidase-enzyme mimic behavior, compared to other previously reported nanomaterials (**Table 1**).

3.5. Colorimetric sensing of Cr(VI)

To further widen the scope of the CuS-BSA nanoenzyme, we have investigated the direct sensing of Cr(VI) using the optimized experimental conditions of TMB oxidation by H_2O_2. Indeed, the catalytic activity of CuS-BSA towards TMB oxidation was enhanced in the presence

of Cr(VI), whereby in a low pH medium (pH=3.9), Cr(VI) induces the decomposition of H_2O_2 into H_2O and O_2 [38], which can readily generate $HO^{\bullet}$ radicals when combined with Cu^{2+} on the surface of CuS-BSA nanocomposite; the reaction of Cr(VI) with H_2O_2 can also generate $HO^{\bullet}$ radicals (Haber Weiss-type reaction), which is favored in acidic medium [44, 45]. Cr(VI) sensing was recorded under various experimental conditions, i.e. in the absence (**Fig. S19**) and presence of H_2O_2 (**Fig. S20**) under the optimized reaction conditions. A good linear relationship (R^2= 0.99372) was obtained for Cr(VI) in the 80-200 µM concentration range in the absence of H_2O_2 **(inset of Fig. 6)**; the limit of detection (LOD) was determined using the following formula (Eq. 4):

$$\text{LOD} = (3\times \text{standard deviation of the blank})/\text{slope of linear regression line} \quad (4)$$

The LOD for Cr(VI) was determined to be 18 µM at a signal-to-noise ratio of 3.

Based on this result, the detection of Cr(VI) was examined in the presence of H_2O_2. **Fig. S20** depicts the absorbance of oxTMB (A654 nm) at various H_2O_2 concentrations, where above 20 mM the catalytic activity of CuS-BSA was not much improved. Therefore, we fixed the concentration of H_2O_2 to 20 mM to determine the LOD of Cr(VI) within the 0.01-50 µM concentration range.

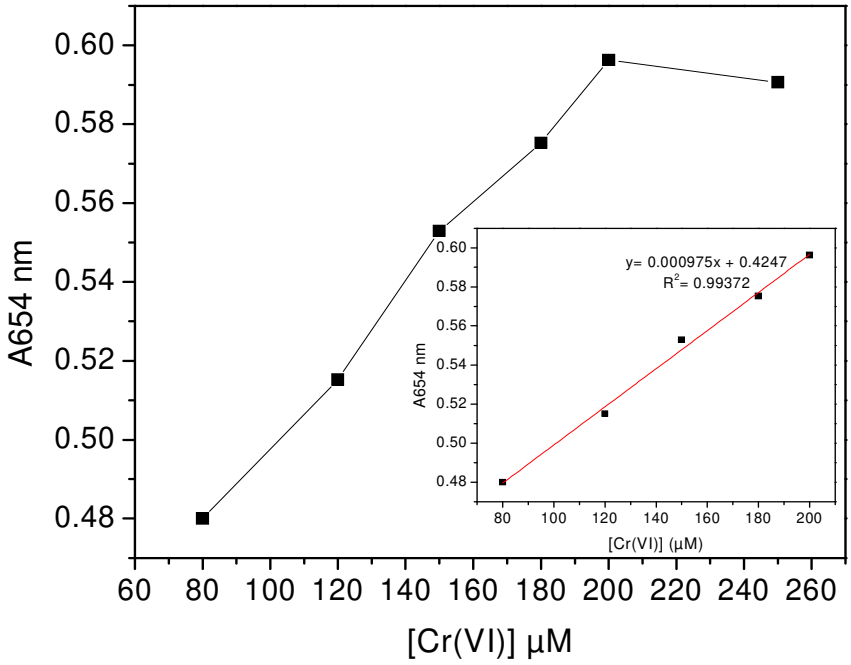

Figure 6: A dose-responsive curve of Cr(VI) using CuS-BSA as a catalyst. Absorbance of oxTMB versus Cr(VI) concentration at 654 nm in the presence of CuS-BSA (0.1 mg/mL), TMB (0.16 mM), pH=3.9, T=25 °C, incubation time=25 min; inset: The linear calibration plot for the determination of Cr(VI).

Noticeably, the LOD of Cr(VI) was enhanced in the presence of H_2O_2 **(Fig. S21)**, and a good linear relation (R^2= 0.9984) between the absorbance A654 nm and the concentration of Cr(VI) within the 0-100 nM and 1-20 µM ranges was observed **(Fig. 7 and Inset of Fig. S21)**. The LOD was found to be 50 nM at a signal-to-noise ratio of 3 using the lower linear range, below the detectable level determined by the U.S EPA (1.9 µM) [46], demonstrating the sensitive detection of Cr(VI) using CuS-BSA nanocomposite.

The performance of the developed sensor is better than that reported for the same metal ion using colorimetric detection scheme (**Table 2**).

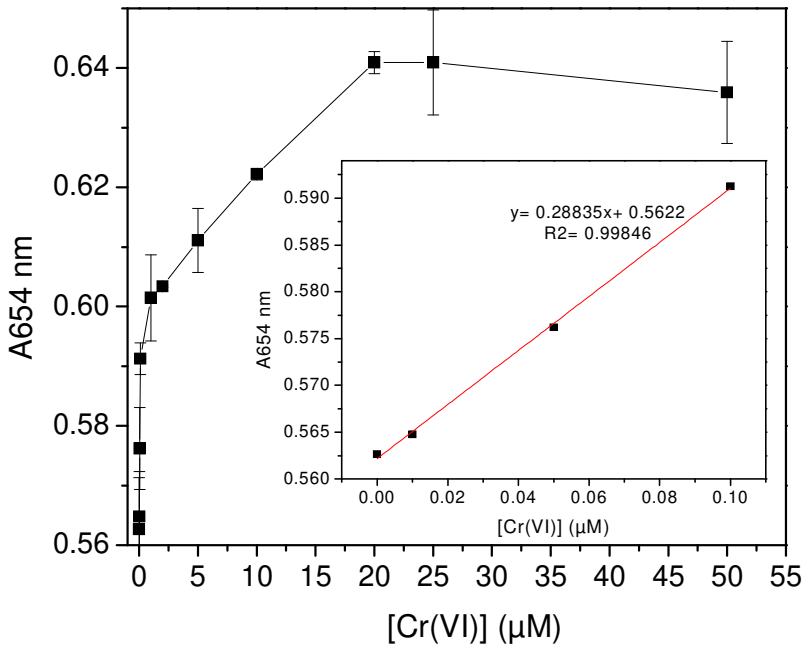

Figure 7: A dose-responsive curve of Cr(VI) using CuS-BSA as a catalyst. Absorbance of oxTMB versus Cr(VI) concentration at 654 nm in the presence of CuS-BSA (0.1 mg/mL), TMB (0.16 mM), H_2O_2 (20 mM), pH=3.9, T=25 °C, incubation time=25 min; inset: The calibration curve in the lower concentration range.

Table 2: Comparison of different nanomaterials for colorimetric sensing of Cr(VI).

Materials	LOD	Linear range	Ref.
GA-Au NPs	2 µM	1-20 µM	[46]
BSA-Au NPs/STCP	280 nM	0.5-50.0 µM	[47]
frGO-Cu	67.13 nM	0-200 nM	[48]
CuS-BSA	50 nM and 6.8 µM	0-100 nM and 1-20 µM	Our work

3.6. Analysis of hydroxyl radicals (HO•)

To better understand the mechanism of TMB oxidation, a probe molecule, terephthalic acid (TA), was used to confirm the generation of HO• radicals; this molecule can react with HO• radicals to produce a fluorescent molecule, 2-hydroxyterephthalic acid (HTA), which exhibits a fluorescence emission band with a maximum at 430 nm under an excitation at 315 nm. **Fig. 8** depicts the evolution of fluorescence emission intensity under various experimental conditions, where the highest intensity was recorded for the reaction containing CuS-BSA, H_2O_2, Cr(VI) and TA, indicating that H_2O_2 decomposition was enhanced in the presence of Cr(VI).

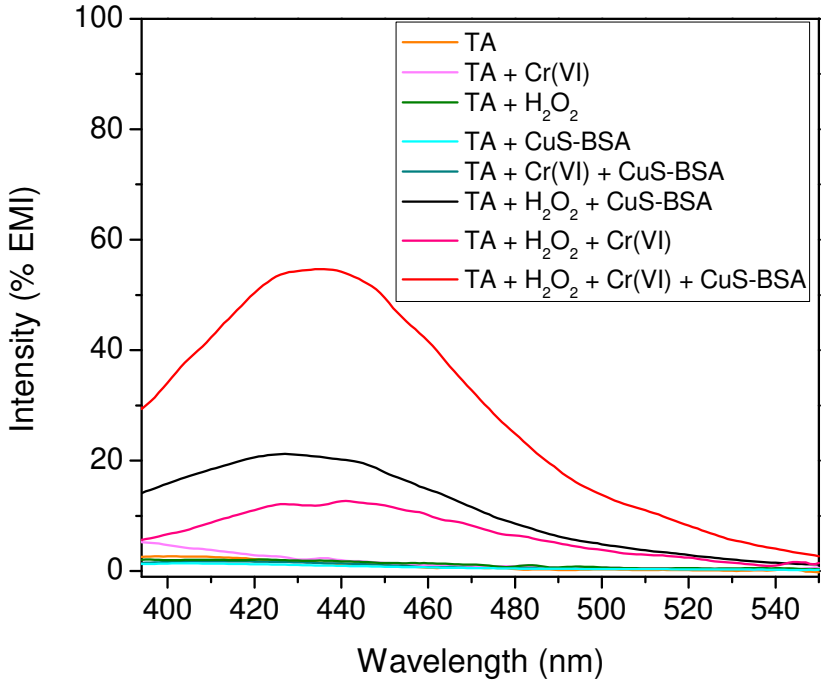

Figure 8: Fluorescence spectra to identify hydroxyl radicals' formation using terephthalic acid (TA) as a fluorescent probe. Reaction conditions: CuS-BSA (0.1 mg/mL), H_2O_2 (20 mM), Cr(VI) (20 µM), TA (0.15 mM) and 0.1 M acetate buffer (pH = 3.9) for 25 min at 25 °C.

3.7. Detection of Cr(VI) in real environmental water samples

To validate the practical application of our proposed enzyme mimic, Cr(VI) detection was tested in different environmental samples using the optimized conditions (CuS-BSA (0.1

mg/mL), H_2O_2 (20 mM), TMB (0.16 mM), T=25°C, t=25 min). In brief, various concentration of Cr(VI) (10, 50, 100 nM) were spiked into real water samples collected from different areas in France. The Cr(VI) concentration present in real water samples was determined from a calibration curve, which was established at 654 nm using a series of Cr(VI) concentrations under the same procedure discussed above. The percentage recovery ($[Cr(VI)]_{found}/[Cr(VI)]_{added} \times 100$) and relative standard deviation (RSD %) in these water samples are listed in **Table 3** (n=3). As shown in **Table 3**, the CuS-BSA nanocomposite displayed good recovery percentage for Cr(VI) sensing in different environmental water samples.

Table 3: Detection of Cr(VI) in real environmental water samples (n=3).

Samples	**Cr(VI) added (nM)**	**Cr(VI) found (nM)**	**Recovery (%)**	**RSD (%)**
Tap water	10	9.95	99.5	0.71
	50	49.5	99	1.42
	100	96	96	2.94
Pond water	10	9.6	96.3	5.79
	50	49.3	98.6	1.24
	100	97.6	97.6	0.59
Sea water	10	9	90	15.7
	50	49.5	99	1.4
	100	92	92	3.07
Tube-well water	10	9.2	96.5	5.12
	50	49	98	5.7
	100	98.5	98.5	0.71

3.8. Selectivity and reproducibility of CuS-BSA enzyme-mimic for sensing heavy metal Cr(VI) ions

In order to evaluate the selectivity of CuS-BSA, the absorbance (A=654 nm) was monitored in presence of different interfering ions (Na^{+}, Hg^{2+}, Zn^{2+}, Co^{2+}, Ni^{2+}, Cr^{3+}) under the same conditions using 5-times higher concentration than the optimized Cr(VI) concentration. The specificity of our sensor was tested with the same experimental procedure as mentioned above. As can be seen from **Fig. 9**, Cr(VI) showed the highest remarkable response, indicating the good selectivity of the developed sensor. Interestingly, the absorbance was not enhanced much, even when the concentration of the interfering ions was 5 times higher (100 µM) than that of Cr(VI) (**Fig. S22**). Also, in the absence of H_2O_2, the interfering ions did not induce blue color change. Notably, due to the higher redox potential of Cr^{6+}/Cr^{3+} (E= +1.33 V) [49] among other interfering metal ions, Na^{+}/Na (-2.71 V), Co^{2+}/Co (-0.28 V), Zn^{2+}/Zn (-0.76 V), Ni^{+}/Ni (-0.36 V), Hg^{2+}/Hg (E= +0.92 V), Cr^{3+}/Cr (-0.74 V), it acts as a strong oxidizing agent in an acidic environment for the dismutation of H_2O_2 [7]. Therefore, the results demonstrated high specificity, sensitivity, selectivity, and colorimetric assay can be achieved using CuS-BSA nanocomposite for Cr(VI) detection.

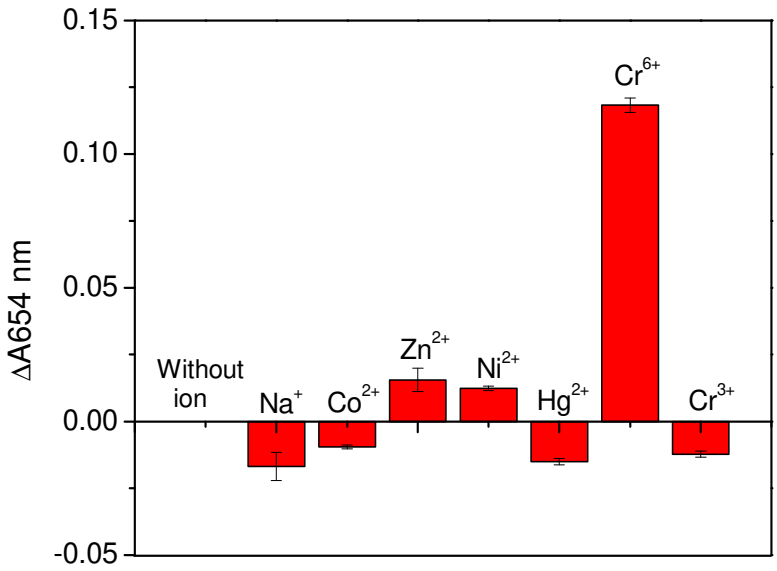

Figure 9: UV-vis absorption at 654 nm of oxTMB in the presence of different interfering ions of concentration 20 µM. Reaction conditions: CuS-BSA (0.1 mg/mL), H_2O_2 (20 mM), TMB (0.16 mM), Cr(VI) (20 µM) and 0.1 M acetate buffer (pH = 3.9), T=25 °C, incubation time=25 min.

The reusability of CuS-BSA as an enzyme-mimic for TMB oxidation was investigated by performing the reaction for four repeated cycles. As shown in **Fig. 10**, the relative activity was approximately the same after four catalytic cycles with a relative STD of 2.8%. The result indicates that CuS-BSA nanocomposite is an enzyme-mimic with excellent catalytic activity and stability.

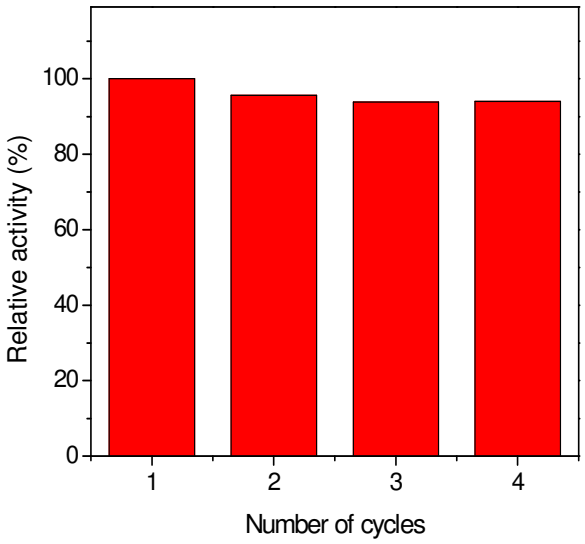

Figure 10: Catalytic activity of CuS-BSA nanocomposite for four successive repeated cycles.

4. Conclusion

In summary, this work presented a simple and cost-effective method for the synthesis of CuS-BSA nanocomposite with peroxidase-like activity towards the catalytic oxidation of TMB. The enhanced activity of the nanoenzyme was further applied for the sensitive and selective detection of hexavalent chromium ions. The proposed sensor showed that the catalytic reaction follows typical Michaelis–Menten kinetics in a pH-dependent manner. Under optimized experimental conditions, a good linear calibration plot was obtained in the concentration range of 0–100 nM

and 1-20 µM of Cr(VI) with a detection limit of 50 nM using the lower linear range. Using terephthalic acid, it was possible to confirm the generation of HO• radicals during the TMB catalytic oxidation by H_2O_2 in the presence of CuS-BSA, a process that has been enhanced in the presence of Cr(VI). The method was effectively tested for the determination of Cr(VI) content in spiked real environmental water samples. Based on these observations, the CuS-BSA nanocomposite showed better performance over natural enzymes which opened new promising applications in many fields.

Acknowledgement

AS, AB, SS and RB acknowledge financial support from the Centre National de la Recherche Scientifique (CNRS), the University of Lille, the Hauts-de-France region and the CPER "Photonics for Society".

References

[1] R.A. Anderson, Chromium, glucose intolerance and diabetes, Am. J. Clin. Nutr. 17 (1998) 548-555.

[2] K.N. Jeejeebhoy, R. Chu, E. Marliss, G.R. Greenberg, A. Bruce-Robertson, Chromium deficiency, glucose intolerance, and neuropathy reversed by chromium supplementation, in a patient receiving long-term total parenteral nutrition, Am. J. Clin. Nutr. 30 (1977) 531-538.

[3] F.-M. Li, J.-M. Liu, X.-X. Wang, L.-P. Lin, W.-L. Cai, X. Lin, et al., Non-aggregation based label free colorimetric sensor for the detection of Cr(VI) based on selective etching of gold nanorods, Sens. Actuators B 155 (2011) 817-822.

[4] L. Blade, M.S. Yencken, M. Wallace, J. Catalano, A. Khan, J. Topmiller, et al., Hexavalent chromium exposures and exposure-control technologies in American enterprise: results of a NIOSH field research study, J. Occup. Environ. Hyg. 4 (2007) 596-618.

[5] U. EPA, Toxicological review of hexavalent chromium, Washington, DC: U, (1998).

[6] X. Shi, Y. Mao, A.D. Knapton, M. Ding, Y. Rojanasakul, P.M. Gannett, et al., Reaction of Cr (VI) with ascorbate and hydrogen peroxide generates hydroxyl radicals and causes DNA damage: role of a Cr(IV)-mediated Fenton-like reaction, Carcinogenesis 15 (1994) 2475-2478.

[7] J.F. Perez-Benito, C. Arias, A Kinetic Study of the Chromium (VI)− Hydrogen Peroxide Reaction. Role of the Diperoxochromate (VI) Intermediates, J. Phys. Chem. A 101 (1997) 4726-4733.

[8] P.A. Glasser, Kinetics and Mechanisms of Cr 6+ Reduction by Structural Fe(II) in Clay Minerals: Miami University; 2014.

[9] U. EPA, Guidelines for Carcinogen Risk Assessment US Environmental Protection Agency, Washington, DC, EPA/630/P-03/001F, (2005).

[10] A.S. Trindade, A.F. Dantas, D.C. Lima, S.L. Ferreira, L.S. Teixeira, Multivariate optimization of ultrasound-assisted extraction for determination of Cu, Fe, Ni and Zn in vegetable oils by high-resolution continuum source atomic absorption spectrometry, Food Chem. 185 (2015) 145-150.

[11] V.N. Losev, O.V. Buyko, A.K. Trofimchuk, O.N. Zuy, Silica sequentially modified with polyhexamethylene guanidine and Arsenazo I for preconcentration and ICP–OES determination of metals in natural waters, Microchem. J. 123 (2015) 84-89.

[12] H. Wang, Z. Wu, B. Chen, M. He, B. Hu, Chip-based array magnetic solid phase microextraction on-line coupled with inductively coupled plasma mass spectrometry for the determination of trace heavy metals in cells, Analyst 140 (2015) 5619-5626.

[13] L. Gao, J. Zhuang, L. Nie, J. Zhang, Y. Zhang, N. Gu, et al., Intrinsic peroxidase-like activity of ferromagnetic nanoparticles, Nat. Nanotechnol. 2 (2007) 577.

[14] D.P. Cormode, L. Gao, H. Koo, Emerging biomedical applications of enzyme-like catalytic nanomaterials, Trends Biotechnol. 36 (2018) 15-29.

[15] C. Coughlan, M. Ibanez, O. Dobrozhan, A. Singh, A. Cabot, K.M. Ryan, Compound copper chalcogenide nanocrystals, Chem. Rev. 117 (2017) 5865-6109.

[16] Y. Zhao, L. Jiang, Hollow micro/nanomaterials with multilevel interior structures, Adv. Mater. 21 (2009) 3621-3638.

[17] P. Huang, Z. Li, H. Hu, D. Cui, Synthesis and characterization of bovine serum albumin-conjugated copper sulfide nanocomposites, J. Nanomater. 2010 (2010) 33.

[18] T. Yang, Y. Wang, H. Ke, Q. Wang, X. Lv, H. Wu, et al., Protein-Nanoreactor-Assisted Synthesis of Semiconductor Nanocrystals for Efficient Cancer Theranostics, Adv. Mater. 28 (2016) 5923-5930.

[19] L. Yang, R. Xing, Q. Shen, K. Jiang, F. Ye, J. Wang, et al., Fabrication of protein-conjugated silver sulfide nanorods in the bovine serum albumin solution, J. Phys. Chem. B 110 (2006) 10534-10539.

[20] C. Pradier, F. Karman, J. Telegdi, E. Kalman, P. Marcus, Adsorption of Bovine Serum Albumin on Chromium and Molybdenum Surfaces Investigated by Fourier-Transform Infrared Reflection− Absorption Spectroscopy (FT-IRRAS) and X-ray Photoelectron Spectroscopy, J. Phys. Chem. B 107 (2003) 6766-6773.

[21] G. Iucci, G. Polzonetti, G. Infante, L. Rossi, XPS and FT-IR spectroscopy study of albumin adsorption on the surface of a π-conjugated polymer film, Surf. Interface Anal. 36 (2004) 724-728.

[22] X. Gong, Y. Bi, Yihua Zhao, G. Liu, W. Y. Teoh, Graphene oxide-based electrochemical sensor: a platform for ultrasensitive detection of heavy metal ions, RSC Adv. 4 (2014) 24653-24657.

[23] A. Belatik, S. Hotchandani, R. Carpentier, H.-A. Tajmir-Riahi, Locating the binding sites of Pb (II) ion with human and bovine serum albumins, PLoS One 7 (2012) e36723.

[24] J. Mahmood, E.K. Lee, M. Jung, D. Shin, H.-J. Choi, J.-M. Seo, et al., Two-dimensional polyaniline (C_3N) from carbonized organic single crystals in solid state, Proc. Natl. Acad. Sci. 113 (2016) 7414-7419.

[25] A. Escudeiro, T. Polcar, A. Cavaleiro, Adsorption of bovine serum albumin on Zr co-sputtered aC (: H) films: implication on wear behaviour, J. Mech. Behav. Biomed. Mater. 39 (2014) 316-327.

[26] Y. Zhou, Y. Bai, H. Liu, X. Jiang, T. Tong, L. Fang, et al., Tellurium/Bovine Serum Albumin Nanocomposites Inducing the Formation of Stress Granules in a Protein Kinase R-Dependent Manner, ACS Appl. Mater. Interfaces 10 (2018) 25241-25251.

[27] E. Ieva, A. Trapani, N. Cioffi, N. Ditaranto, A. Monopoli, L. Sabbatini, Analytical characterization of chitosan nanoparticles for peptide drug delivery applications, Anal. Bioanal. Chem. 393 (2009) 207-215.

[28] K. Jeon, Synthesis and Characterization of Thionated Reduced Graphene Oxides and Their Thin Films: Arizona State University; 2013.

[29] Z. Luo, S. Lim, Z. Tian, J. Shang, L. Lai, B. MacDonald, et al., Pyridinic N doped graphene: synthesis, electronic structure, and electrocatalytic property, J. Mater. Chem. 21 (2011) 8038-8044.

[30] S. Liu, J. Tian, L. Wang, Y. Zhang, X. Qin, Y. Luo, et al., Hydrothermal treatment of grass: a low-cost, green route to nitrogen-doped, carbon-rich, photoluminescent polymer nanodots as an effective fluorescent sensing platform for label-free detection of Cu (II) ions, Adv. Mater. 24 (2012) 2037-2041.

[31] J. Zhang, J. Yu, Y. Zhang, Q. Li, J.R. Gong, Visible light photocatalytic H_2-production activity of CuS/ZnS porous nanosheets based on photoinduced interfacial charge transfer, Nano Lett. 11 (2011) 4774-4779.

[32] J. Qian, K. Wang, Q. Guan, H. Li, H. Xu, Q. Liu, et al., Enhanced wet hydrogen peroxide catalytic oxidation performances based on CuS nanocrystals/reduced graphene oxide composites, Appl. Surf. Sci. 288 (2014) 633-640.

[33] I. Ancutiene, J.G. Navea, J. Baltrusaitis, Structural, chemical and optical properties of the polyethylene–copper sulfide composite thin films synthesized using polythionic acid as sulfur source, Appl. Surf. Sci. 347 (2015) 520-527.

[34] P. Borthakur, P.K. Boruah, G. Darabdhara, P. Sengupta, M.R. Das, A.I. Boronin, et al., Microwave assisted synthesis of CuS-reduced graphene oxide nanocomposite with efficient photocatalytic activity towards azo dye degradation, J. Environ. Chem. Eng. 4 (2016) 4600-4611.

[35] L. Liang, S. Peng, Z. Yuan, C. Wei, Y. He, J. Zheng, et al., Biocompatible tumor-targeting nanocomposites based on CuS for tumor imaging and photothermal therapy, RSC Adv. 8 (2018) 6013-6026.

[36] X. Chen, L. Ding, P. Liu, Q. Wang, Synthesis of protein-assisted aqueous Ag_2S quantum dots in the bovine serum albumin solution, Surf Interface Anal. 46 (2014) 301-306.

[37] S. Yadav, P. Bajpai, Synthesis of copper sulfide nanoparticles: pH dependent phase stabilization, Nano-Structures & Nano-Objects 10 (2017) 151-158.

[38] P. Borthakur, P.K. Boruah, M.R. Das, S.B. Artemkina, P.A. Poltarak, V.E. Fedorov, Metal free MoS 2 2D sheets as a peroxidase enzyme and visible-light-induced photocatalyst towards detection and reduction of Cr (VI) ions, New J. Chem. 42 (2018) 16919-16929.

[39] W. He, H. Jia, X. Li, Y. Lei, J. Li, H. Zhao, et al., Understanding the formation of CuS concave superstructures with peroxidase-like activity, Nanoscale 4 (2012) 3501-3506.

[40] H. Liu, M. Jiao, C. Gu, M. Zhang, Au@Cu_xOS yolk-shell nanomaterials with porous shells act as a new peroxidase mimic for the colorimetric detection of H_2O_2, J. Alloys Compd. 741 (2018) 197-204.

[41] Q. Zhang, M. Li, C. Guo, Z. Jia, G. Wan, S. Wang, et al., Fe_3O_4 Nanoparticles Loaded on Lignin Nanoparticles Applied as a Peroxidase Mimic for the Sensitively Colorimetric Detection of H_2O_2, Nanomaterials 9 (2019) 210.

[42] G. Darabdhara, B. Sharma, M.R. Das, R. Boukherroub, S. Szunerits, Cu-Ag bimetallic nanoparticles on reduced graphene oxide nanosheets as peroxidase mimic for glucose and ascorbic acid detection, Sens. Actuators B 238 (2017) 842-851.

[43] H.-F. Lu, J.-Y. Li, M.-M. Zhang, D. Wu, Q.-L. Zhang, A highly selective and sensitive colorimetric uric acid biosensor based on Cu (II)-catalyzed oxidation of 3,3′,5,5′-tetramethylbenzidine, Sens. Actuators B 244 (2017) 77-83.

[44] A.D. Bokare, W. Choi, Chromate-induced activation of hydrogen peroxide for oxidative degradation of aqueous organic pollutants, Environ. Sci. Technol. 44 (2010) 7232-7237.

[45] X. Shi, Reduction of chromium (VI) and its relationship to carcinogenesis, J. Toxicol. Environ. Health Part B: Critical Reviews 2 (1999) 87-104.

[46] C. Dong, G. Wu, Z. Wang, W. Ren, Y. Zhang, Z. Shen, et al., Selective colorimetric detection of Cr (III) and Cr (VI) using gallic acid capped gold nanoparticles, Dalton Trans. 45 (2016) 8347-8354.

[47] J.-f. Guo, D.-q. Huo, M. Yang, C.-j. Hou, J.-j. Li, H.-b. Fa, et al., Colorimetric detection of Cr (VI) based on the leaching of gold nanoparticles using a paper-based sensor, Talanta 161 (2016) 819-825.

[48] P. Borthakur, P.K. Boruah, M.R. Das, S. Szunerits, R. Boukherroub, Cu(0) nanoparticle-decorated functionalized reduced graphene oxide sheets as artificial peroxidase enzymes: application for colorimetric detection of Cr (VI) ions, New J. Chem. 43 (2019) 1404-1414.

[49] M. Dehghani, B. Heibati, A. Asadi, I. Tyagi, S. Agarwal, V. Gupta, Reduction of noxious Cr (VI) ion to Cr (III) ion in aqueous solutions using H_2O_2 and UV/H_2O_2 systems, J. Ind. Eng. Chem. 33 (2016) 197-200.

Graphical abstract

A CuS-BSA nanocomposite is synthesized and exhibited a peroxidase-enzyme mimic towards the oxidation of 3,3′,5,5′-tetramethylbenzidine (TMB) through the generation of hydroxyl radicals for the rapid, sensitive and selective detection of Cr(VI).